Stability Analysis of the Discrete-Data Large-Space-Telescope System

B. C. Kuo,* G. Singh,†
University of Illinois, Urbana-Champaign, Ill.
and
S. M. Seltzer‡
NASA Marshall Space Flight Center, Ala.

This paper considers the application of the discrete describing function to the stability analysis of the Large-Space Telescope (LST) system. An analytical model of the CMG gimbal friction is derived, which is then used to arrive at a closed-form analtical expression for the discrete describing function of the nonlinearity. The analysis is used for the study of the fine-pointing stability of the LST vehicle. Simulation results corroborate the conclusions from the analytical analysis.

Nomenclature

θ_V = vehicle position (rad)
ω_V = vehicle velocity (rad/sec)
θ_G = gimbal position (rad)
ω_G = gimbal velocity (rad/sec)
T_{GF} = torque output of the nonlinearity (ft-lb)
Error = error input command (rad/sec) to the CMG = $\chi - K_0\theta_V - K_1\omega_V$
K_1 = 9700 ft-lb/rad, (gimball rate loop integral gain)
K_{CLI} = 1.6×10^4 volts/sec/amp, (current loop integral gain)
T_1 = 6.4 millisec, (current loop lead time constant)
T_2 = 0.16 millisec (current loop lag time constant)
J_V = 10^5 ft-lb-sec^2 (vehicle inertia)
H = 600 ft-lb-sec (CMG angular momentum)
J_G = 2.1 ft-lb-sec^2 (gimbal inertia)
I_{OA} = 2.1 ft-lb-sec^2 (CMG output axis inertia)
D_{OA} = 20 ft-lb-sec (CMG output axis damping)
K_{OA} = 10^6 ft-lb (CMG output axis spring constant)
K_0 = 5.75835×10^3 (vehicle controller coefficient)
K_1 = 1.37102×10^3 (vehicle controller coefficient)
K_T = 2.5 ft-lb/amp (torque motor sensitivity)
K_B = 3.4 volts/rad/sec (torque motor back emf constant)
R_m = 4.4 ohms (torque armature resistance)
T_E = 6.4 millisec (torque motor armature time constant)
K_p = 2.6 ft-lb/rad/sec (gimbal rate loop proportional gain)

I. Introduction

THE Large Space Telescope (LST) is an orbiting astronomical observatory which is scheduled for launching by NASA in the next decade.[1] It will be the first large payload of the space shuttle program and is expected to have an orbit approximately 500 miles above the surface of the earth.

Free from all atmospheric disturbances, the LST is expected to provide valuable information regarding stars up to the 15th magnitude. Star observation experiments are expected to last for several hours, and during this time, the LST vehicle is required to maintain its position within 0.005 arc-sec (2.42×10^{-8} arc-radians). A fine-pointing control system will be used to provide the pointing accuracy during the periods of the experiments. Control torques are provided by three control-moment gyroscopes (CMG) located on the vehicle.

Received June 13, 1975; revision received January 14, 1976. This work was supported by NASA contract NAS8-29853.
Index category: Spacecraft Attitude Dynamics and Control.
*Professor of Electrical Engineering. Member AIAA.
†Senior Research Engineer. Member AIAA.
‡Chief, Pointing Control Systems Branch, Systems Dynamics Laboratory. Associate Fellow AIAA.

This paper is concerned with the stability studies of the discrete-data version of the LST with its fine-pointing control system. In particular, the existence of stable limit cycles due to the CMG gimbal friction nonlinearity has been analyzed.

By utilizing some recent results of solid friction studies,[2,3] an analytical model for the CMG gimbal friction is derived. This allows the application of the discrete describing function techniques[4,5] to the stability study of the LST system.

As in the continuous-data case,[6] it is found that stable limit cycles can exist depending upon the system parameters and the characteristics of the nonlinearity. In addition, the sampling period is found to play a dominant role in the characteristics of the oscillations.

II. LST System Model

A single-axis model of the LST with the fine-pointing control system is shown in Fig. 1. The vehicle is represented by a single inertia J_V (G_7 in Fig. 1) without any bending modes. Studies are presently underway to determine a LST vehicle model which, while including the effects of the dominant bending modes, will still be analytically tractable. The results of this paper will be applicable to more complex models without difficulties.

The CMG is also modeled as a single inertia element J_G (G_6) with its complete control loop. Blocks G_2 and G_3 represent the gimbal controller, while G_4 represents the current amplifier. The torque motor is represented by its armature dynamics as G_5, and its torque and induced EMF constants, K_T and K_B, respectively. Block G_8 represents the torsional feedback of the CMG output axis, and N represents the CMG gimbal friction nonlinearity. The characteristics of the nonlinearity are described in detail in Sec. III.

The block, G_1, represents the vehicle controller which is of the proportional-plus-derivative type. This controller is used here to illustrate the stability analysis method described in this paper. It can be shown that this controller is optimal in the sense of pole-placement design without the nonlinearity, and simulation results show that the system response is quite good. However, the analytical results of this paper are applicable to controllers of other configurations, and, therefore, the particular choice of G_1 is inconsequential.

III. Modeling of the CMG Frictional Nonlinearity

One of the major difficulties in the modeling of the dynamics of the CMG is in the accurate representation of the nonlinear gimbal friction characteristics. The running friction of the gimbal axis consists of both tachometer brush friction and the hysteresis drag which is associated with the brushless

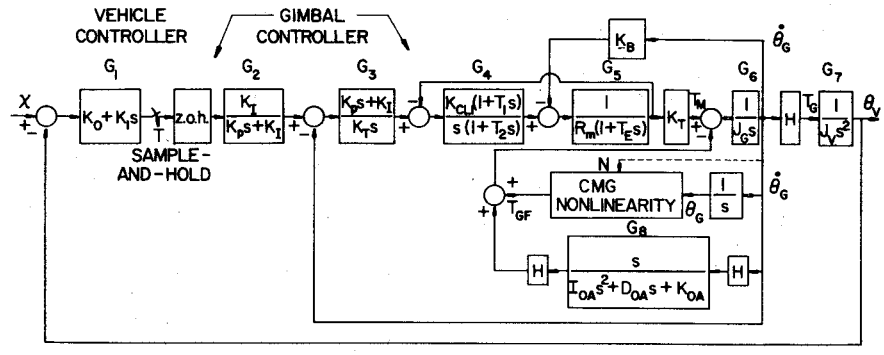

Fig. 1 A dynamic model for the LST system with the complete CMG control loop.

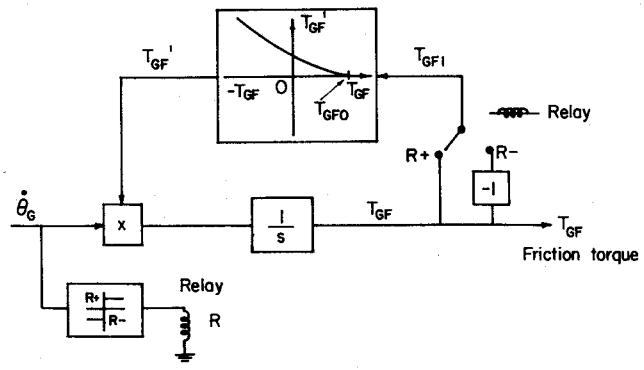

Fig. 2 A simulation block diagram of the CMG friction nonlinearity.

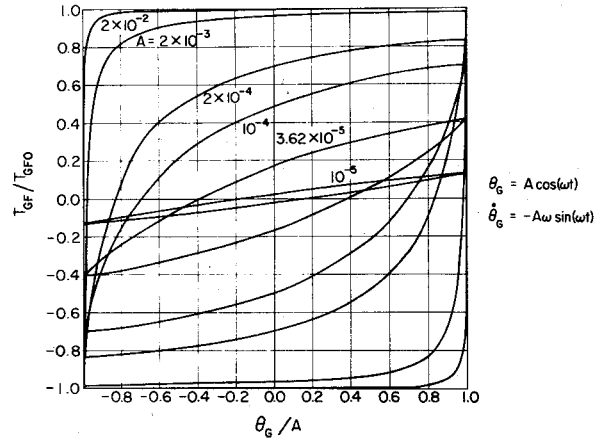

Fig. 3 Normalized frictional torque vs θ_{IG}/A for CMG nonlinearity with cosine function input.

dc permanent-magnet torque motor. These frictional torques do not have significant effect on large motion gimbal-rate control-loop performance other than the power loss required to overcome the drag torque. However, the accurate representation of these torques for small motion has a very pronounced influence on the gimbal-rate control-loop small-motion performance. Therefore, for fine-pointing studies, the accurate modeling of these torques is essential in predicting the existence of stiction limit cycles and the control-loop response to very low-level commands.

While common nonlinear frictional models, usually of the Coulomb type, are adequate for large-signal studies, they are inappropriate for signals with extremely small amplitudes. In this section, a more rigorous mathematical model of the CMG friction nonlinearity is derived.

It was reported from experimental studies[2] that the frictional characteristics of the CMG are very closely represented by the solid friction simulating model reported in the literature.[3] In this simulator, advantage is taken of the observation that the frictional torque, T_{GF}, being a function of displacement, θ_G, can be differentiated with respect to time. Thus,

$$\frac{dT_{GF}}{dt} = \frac{dT_{GF}}{d\theta_G} \cdot \frac{d\theta_G}{dt} = T'_{GF}\dot{\theta}_G \tag{1}$$

Then T_{GF} can be generated by integrating both sides of Eq. (1) with respect to t. It is observed that T'_{GF} is easily found as a function of θ_G, and the simulation model actually has T'_{GF} generated by a function generator with T_{GF} as the input. The simulation block diagram for the CMG friction nonlinearity is shown in Fig. 2. Notice that this model has $\dot{\theta}_G$ as input and T_{GF} as the output.

Referring to Fig. 1, the block diagram of Fig. 2 may replace the blocks for the simplified nonlinearity between $\dot{\theta}_G$ and T_{GF}.

It has been demonstrated experimentally[3] that for solid rolling friction, the relation between T'_{GF} and T_{GF} may be approximated by a square-law expression,

$$T'_{GF} = \frac{dT_{GF}}{d\theta_G} = \gamma(T_{GF} - T_{GFO})^2 \quad T_{GF} \le T_{GFO} \tag{2}$$

$$T'_{GF} = 0 \qquad T_{GF} > T_{GFO} \tag{3}$$

where γ is a positive constant. However, for the CMG friction, the frictional torque is also velocity dependent, as shown in Fig. 2. Therefore, Eq. (2) should be written

$$T'_{GF} = \gamma(T_{GFI} - T_{GFO})^2 \tag{4}$$

$$T_{GFI} = T_{GF}SGN(\dot{\theta}_G) \tag{5}$$

For simulation purpose, the block diagram of Fig. 2 can be easily programmed on the digital computer, and the program can be used for any input.

Equation (4) can also be integrated with respect to θ_G directly to yield

$$T_{GF} = \frac{(\theta_G - \theta_{Gi})\gamma(T_{GFi} - T_{GFO})T_{GFO} - T_{GFi}}{(\theta_G - \theta_{Gi})\gamma(T_{GFi} - T_{GFO}) - 1} \quad \dot{\theta}_G \ge 0 \tag{6}$$

$$T_{GF} = \frac{-(\theta_G - \theta_{Gi})\gamma(T_{GFi} + T_{GFO})T_{GFO} - T_{GFi}}{(\theta_G - \theta_{Gi})\gamma(T_{GFi} + T_{GFO}) - 1} \quad \dot{\theta}_G \le 0 \tag{7}$$

where

θ_{Gi} = initial value of θ_G

T_{GFi} = initial value of T_{GF}

The expressions for the frictional torque are valid for any arbitrary input θ_G and initial conditions at the beginning of the process. When θ_G changes sign during the process, the proper expression of Eq. (6) or Eq. (7) should be used, and the initial conditions should be appropriately matched at the switching point.

Our objective is to investigate the behavior of the nonlinearity under a sinusoidal excitation, so that the describing frunction method can be applied. Consequently,

with a sinusoidal-type input, $\theta_G(t) = A\cos\omega t$, the steady-state output of the nonlinearity is obtained by solving Eqs. (4) and (5), or by using Eqs. (6) and (7). The results are

$$\frac{T_{GF}}{T_{GFO}} = \frac{\dfrac{R}{R+1} - \dfrac{a}{2}(1-\cos\omega t)}{\dfrac{a}{2}(1-\cos\omega t) + \dfrac{1}{R-1}} \tag{8}$$

which is valid for $2k\pi \le \omega t \le (2k+1)\pi$, $k = 0, 1, 2, \ldots$, or $\dot\theta_G \le 0$, and

$$\frac{T_{GF}}{T_{GFO}} = \frac{\dfrac{R}{R-1} + \dfrac{a}{2}(1-\cos\omega t)}{\dfrac{a}{2}(1-\cos\omega t) + \dfrac{1}{R-1}} \tag{9}$$

which is valid for $\dot\theta_G \ge 0$, or $(2k+1)\pi \le \omega t \le (2k+2)\pi$, $k = 0,1,2,\ldots$, where

$$a = 2\gamma A T_{GFO} \tag{10}$$

$$R = -\frac{1}{a} + \left(\frac{a^2+1}{a^2}\right)^{1/2} \tag{11}$$

For nominal values of $\gamma = 1.38\times10^5$ and $T_{GFO} = 0.1$, the normalized plots of T_{GF} are shown in Figs. 3 and 4. The curves in Fig. 3 show the T_{GF}/T_{GFO} vs θ_G/A characteristics for various values of A, and the curves in Fig. 4 show the T_{GF}/T_{GFO} vs $\dot\theta_G/A\omega$ characteristics for various values of A.

Figure 3 and 4 show that for larger values of A, the frictional torque changes sign more rapidly when the velocity $\dot\theta_G$ changes sign. As A approaches infinity, the nonlinearity behaves similar to Coulomb friction. A similar effect is noticed as γ is increased.

IV. Discrete Describing Function of the CMG Nonlinearity

Figure 5 shows the block diagram of the sampled-data LST system with the torsional dynamics of the CMG output axis, the current amplifier, the armature time constant of the torque motor, and the back emf loop neglected. This approximation is carried out only for the purpose of simplifying the system configuration, but the analysis conducted in the following can be applied to systems of any complexity. In order to carry out the discrete describing function analysis, a sample-and-hold is inserted in front of the CMG nonlinearity as an approximation. It will be shown later that for the range of sampling periods which are practical for this system, the two-sampler model is quite accurate in the prediction of limit cycles. The original system is referred to as the one-sampler model.

With the sample-and-hold added to the nonlinear loop, the CMG nonlinearity is analytically isolated from the linear dynamics of the system.

Let $N(z)$ denote the discrete describing function of the nonlinearity. It can be shown that the determinant of the system in Fig. 5 is

$$1 + N(z)G(z) = 0 \tag{12}$$

where

$$G(z) = z\left[\frac{G_{ho}G_6}{s\Delta_o}\right] - z\left[\frac{G_{ho}G_6G_7G_1}{\Delta_o}\right]z\left[\frac{G_{ho}G_2G_3G_6}{s\Delta_o}\right]$$

$$+ z\left[\frac{G_{ho}G_1G_2G_3G_6G_7}{\Delta_o}\right]z\left[\frac{G_{ho}G_6}{s\Delta_o}\right] + z\left[\frac{G_{ho}G_1G_2G_3G_6G_7}{\Delta_o}\right] \tag{13}$$

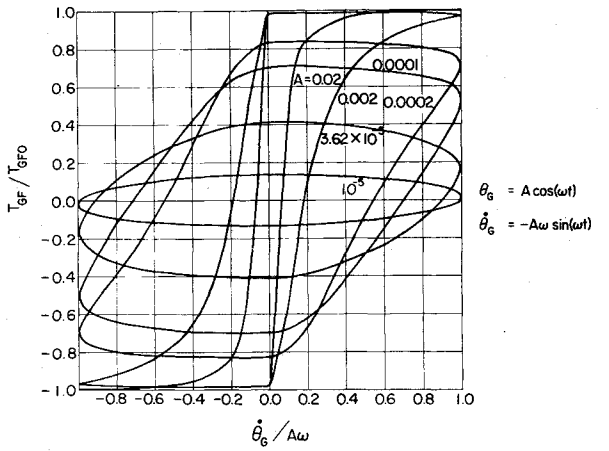

Fig. 4 Normalized frictional torque vs $\theta_G/A\omega$ for CMG nonlinearity with cosine function input.

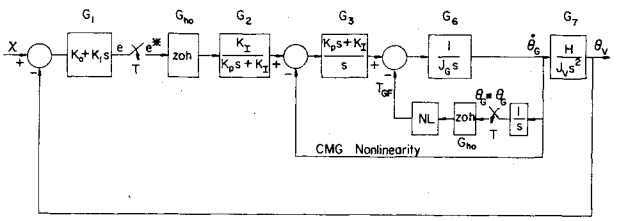

Fig. 5 A block diagram of the simplified LST control system with sampled data.

where z denotes the z-transform operation, and

$$\Delta_o = 1 + G_3G_6 \tag{14}$$

The first step in the derivation of $N(z)$ involves the interchanging of the positions of the nonlinearity and the zero-order hold in Fig. 5. The step is justified since the nonlinearity is amplitude dependent only, so that the signal of T_{GF} is not affected by this interchange.

The second step involves the assumption that θ_G is sinusoidal; that is

$$\theta_G(t) = A\cos(\omega t + \phi) \tag{15}$$

where A, ω, and ϕ denote the amplitude, the frequency in radians, and the phase in degrees of the sinusoid, respectively.

The z-transform of $\theta_G(t)$ is

$$\theta_G(z) = \sum_{k=0}^{\infty} A\cos\left(\frac{2\pi k}{N} + \phi\right)z^{-k} \tag{16}$$

or in closed form,

$$\theta_G(z) = \frac{Az\{[(z-\cos(2\pi/N)]\cos\phi - \sin(2\pi/N)\sin\phi]\}}{z^2 - 2z\cos(2\pi/N) + 1} \tag{17}$$

An important consideration is that because of the periodic nature of the sampler, $\theta_G(t)$, $\theta_G^*(t)$, and $T_{GF}^*(t)$ are all periodic functions of period NT, where N is a positive integer ≥ 2. Therefore, $\omega = 2\pi/NT$, and $\omega T = 2\pi/N$.

The output of the nonlinearity is denoted by $T_{GF}^*(t)$, and its z-transform is $T_{GF}(z)$. The discrete describing function (DDF) of the nonlinearity is defined as

$$N(z) = \frac{T_{GF}(z)}{\theta_G(z)} \tag{18}$$

It turns out that the discrete describing function (DDF) for $N = 2$ must be derived separately, and a general expression for $N(z)$ can be obtained for all $N \ge 3$.

DDF for $N=2$

Let $T_{GF}(kT)$ denote the value of $T^*_{GF}(t)$ at $t=kT$. For $N=2$, the signal $T^*_{GF}(t)$ is a periodic function with a period of $2T$. The z-transform of $T^*_{GF}(t)$ is written

$$T_{GF}(z)=T_{GF}(0)\,(1+z^{-2}+z^{-4}+\ldots)+T_{GF}(T)\,(z^{-1}+z^{-3}+\ldots)=\frac{T_{GF}(0)z^2+T_{GF}(T)z}{z^2-1} \tag{19}$$

For the CMG frictional nonlinearity, it has been established in Eq. (8) that for the sinusoidal input of Eq. (15),

$$T_{GF}(t)=T_{GFO}\frac{\frac{R}{R+1}-\frac{a}{2}[1-\cos(\omega t+\phi)]}{\frac{1}{R+1}+\frac{a}{2}[1-\cos(\omega t+\phi)]} \qquad \dot\theta_G\le 0 \tag{20}$$

$$T_{GF}(t)=T_{GFO}\frac{\frac{R}{R-1}+\frac{a}{2}[1-\cos(\omega t+\phi)]}{\frac{1}{R-1}+\frac{a}{2}[1-\cos(\omega t+\phi)]} \qquad \dot\theta_G\ge 0 \tag{21}$$

Let us introduce the following notation:

$$T_{GF}{}^-(kT)=T_{GF}(t)\,|_{t=kT} \qquad \dot\theta_G\le 0 \tag{22}$$

$$T_{GF}{}^+(kT)=T_{GF}(t)\,|_{t=kT} \qquad \dot\theta_G\ge 0 \tag{23}$$

Substituting $N=2$ into Eq. (17), we have

$$\theta_G(z)=\frac{Az\cos\phi}{z+1} \tag{24}$$

Using Eqs. (18), (19) and (24), the DDF $N(z)$ for $N=2$ is determined.

For stability analysis, we define

$$F(z)=-\frac{1}{N(z)}=\frac{2A\cos\phi}{T_{GF}(T)-T_{GF}(0)} \tag{25}$$

DDF for $N\ge 3$

In general, the z-transform of the output of the nonlinearity may be written as

$$T_{GF}(z)=\sum_{m=0}^{\infty}\sum_{k=0}^{N-1}T_{GF}(kT)z^{-k-mN}=\frac{\sum_{k=0}^{N-1}T_{GF}(kT)z^{N-k}}{z^N-1} \tag{26}$$

Using Eq. (16) for $\theta_G(z)$, the discrete describing function $N(z)$ is written

$$N(z)=\frac{T_{GF}(z)}{\theta_G(z)}=\frac{\sum_{k=0}^{N-1}T_{GF}(kT)z^{N-k}}{(z^N-1)\sum_{k=0}^{\infty}A\cos(\frac{2\pi k}{N}+\phi)z^{-k}} \tag{27}$$

The denominator of $N(z)$ may be simplified as follows

$$\begin{aligned}&(z^N-1)\sum_{k=0}^{\infty}A\cos(\frac{2\pi k}{N}+\phi)z^{-k}\\&=A\sum_{k=0}^{\infty}z^{N-k}\cos(\frac{2\pi k}{N}+\phi)-A\sum_{k=0}^{\infty}z^{-k}\cos(\frac{2\pi k}{N}+\phi)\\&=A\sum_{k=0}^{N-1}\cos(\frac{2\pi k}{N}+\phi)z^{N-k-1}\end{aligned} \tag{28}$$

Thus

$$N(z)=\frac{\sum_{k=0}^{N-1}T_{GF}(kT)z^{N-k-1}}{A\sum_{k=0}^{N-1}\cos(\frac{2\pi k}{N}+\phi)z^{N-k-1}} \qquad (N\ge 3) \tag{29}$$

For $N=3$, $N(z)$ is simplified to

$$N(z)=\frac{T_{GF}(0)z^2+T_{GF}(T)z+T_{GF}(2T)}{A(z-1)\,[(z+0.5)\cos\phi-0.866\sin\phi]} \tag{30}$$

For $N>3$

$$N(z)=\frac{\sum_{k=0}^{N-1}T_{GF}(kT)z^{N-k-1}}{A(z-1)\sum_{k=2}^{N-2}(z-e^{j2\pi k/N})\,[(z-\cos\frac{2\pi}{N})\cos\phi-\sin\frac{2\pi}{N}\sin\phi]} \tag{31}$$

where in general

$$\begin{aligned}T_{GF}(kT)&=T^-_{GF}(kT) \qquad 0<\frac{2\pi k}{N}+\phi<\pi\\&=T^+_{GF}(kT) \qquad \pi<\frac{2\pi k}{N}+\phi<2\pi\end{aligned} \tag{32}$$

where $0\le(2\pi k/N+\phi)\le 2\pi$ must be satisfied by appropriate conversion of the angle $2\pi k/N+\phi$.

For stability studies, the critical regions of $F(z)=-1/N(z)$ should be constructed for $N=2,3,\ldots$, with ϕ varied from 0° to 360°, and A from 0 to infinity. The intersect of the $G(z)$ locus with the critical regions of $-1/N(z)$ represents the satisfaction of Eq. (12) and the condition of self-sustained oscillation excited by some initial conditions.

The following theorems on the properties of $-1/N(z)$ are useful for simplifying the task of the construction of the critical regions. The proofs of these theorems are given elsewhere.[7]

Theorem 1. *For any integral N, the magnitude and phase of $-1/N(z)$ repeat for every $\phi=2\pi/N$ radians.*

Theorem 2. *For odd $N(N\ge 3)$, the magnitude and phase of $-1/N(z)$ repeat for every $\phi=\pi/N$.*

The significance of the last two theorems is that the critical regions of $-1/N(z)$ need be computed only for $0°<\phi\le\pi/N$ for odd N, and $0°<\phi\le 2\pi/N$ for even N.

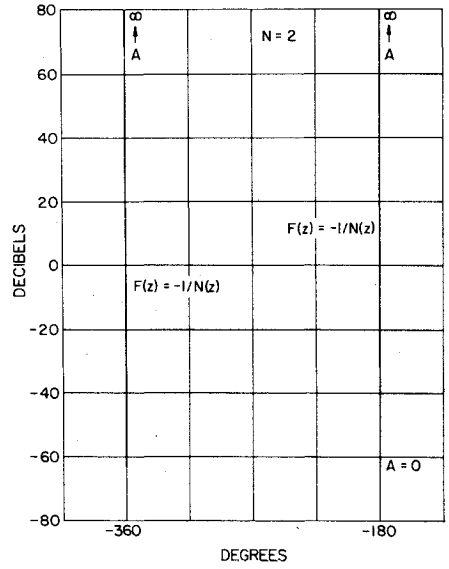

Fig. 6 Discrete describing function plot of CMG frictional nonlinearity, $\gamma=1.38\times10^5$, $N=2$.

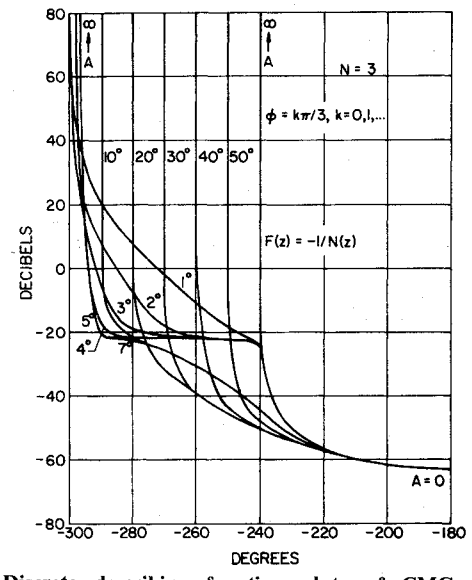

Fig. 7 Discrete describing function plots of CMG frictional nonlinearity, $\gamma = 1.38 \times 10^5$, $N = 3$.

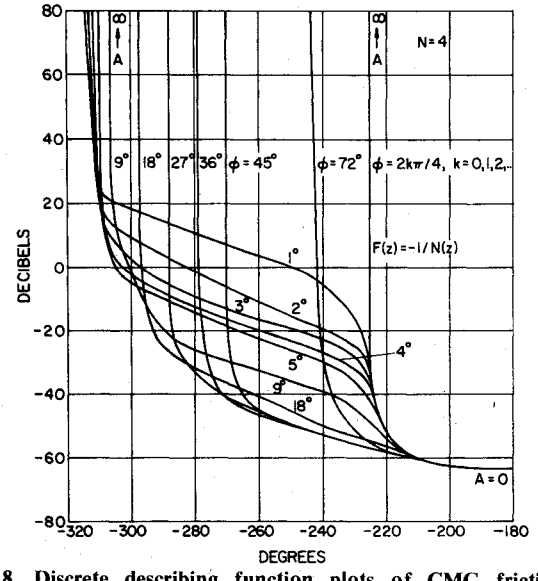

Fig. 8 Discrete describing function plots of CMG frictional nonlinearity, $\gamma = 1.38 \times 10^5$, $N = 4$.

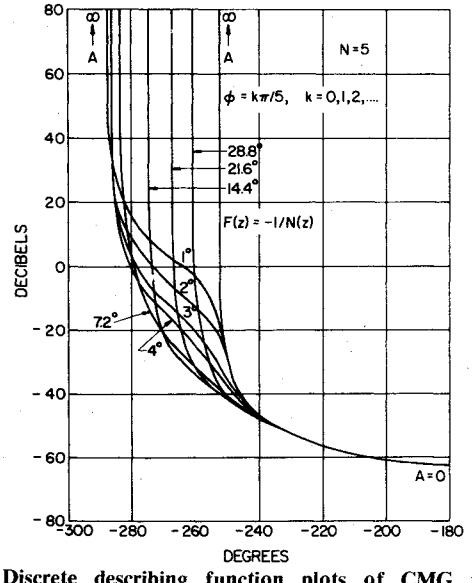

Fig. 9 Discrete describing function plots of CMG frictional nonlinearity, $\gamma = 1.38 \times 10^5$, $N = 5$.

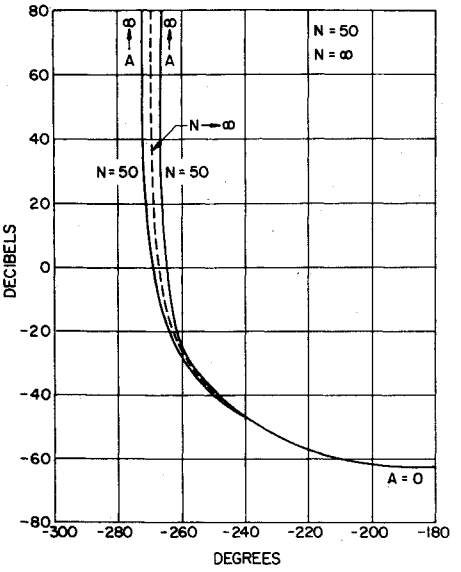

Fig. 10 Discrete describing function plots which form the critical region of the CMG frictional nonlinearity, $\gamma = 1.38 \times 10^5$, $N = 50$ and $N = \infty$.

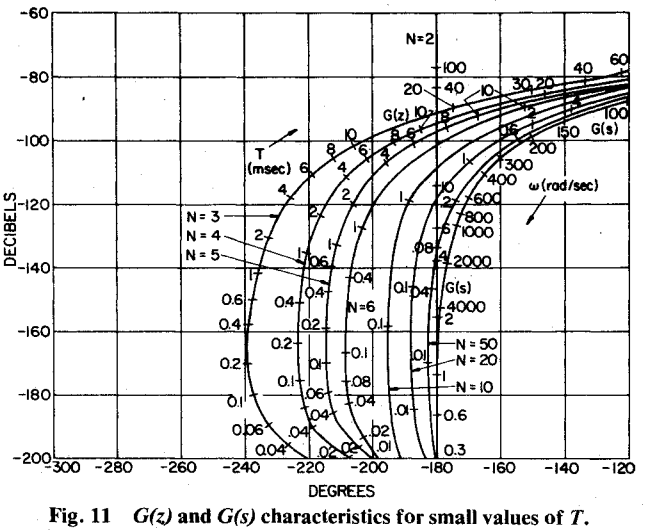

Fig. 11 *G(z)* and *G(s)* characteristics for small values of *T*.

Theorem 3. *Asymptotic behavior of* $-1/N(z)$ *as A approaches infinity.*

a) $$\lim_{A\to\infty} |-1/N(z)| = \infty \tag{33}$$

b) for even $N \geq 4$, $0 < \phi \leq 2\pi/N$.

$$\lim_{A\to\infty} \operatorname{Arg}[-1/N(z)] = \left(\frac{1}{2} - \frac{1}{N}\right)\pi + \phi \tag{34}$$

for odd $N > 3$, $0 < \phi \leq \pi/N$.

$$\lim_{A\to\infty} \operatorname{Arg}[-1/N(z)] = \left(1 - \frac{1}{N}\right)\frac{\pi}{2} + \phi \tag{35}$$

c) for $N = 2$ $0 < \phi \leq \pi$

$$\lim_{A\to\infty} \operatorname{Arg}[-1/N(z)] = 0^\circ \quad 0 < \phi \leq \pi/2$$
$$= \pi \quad \pi/2 < \phi \leq \pi \tag{36}$$

d) for $N = 3$, $0 < \phi \leq \pi/3$

$$\lim_{A\to\infty} \operatorname{Arg}[-1/N(z)] = -5\pi/3 + \phi \tag{37}$$

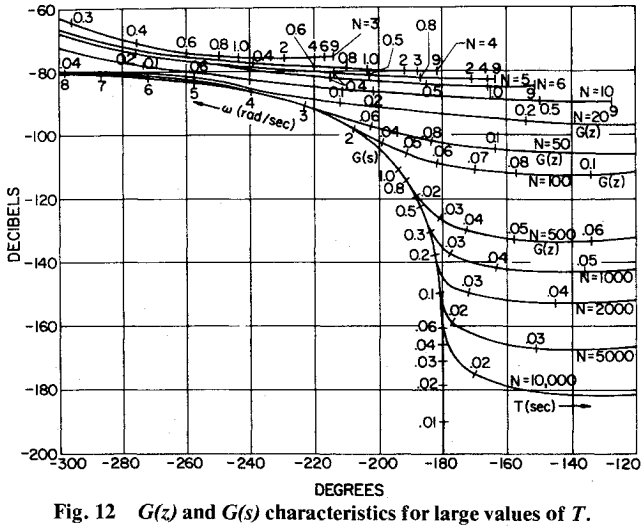

Fig. 12 *G(z)* and *G(s)* characteristics for large values of *T*.

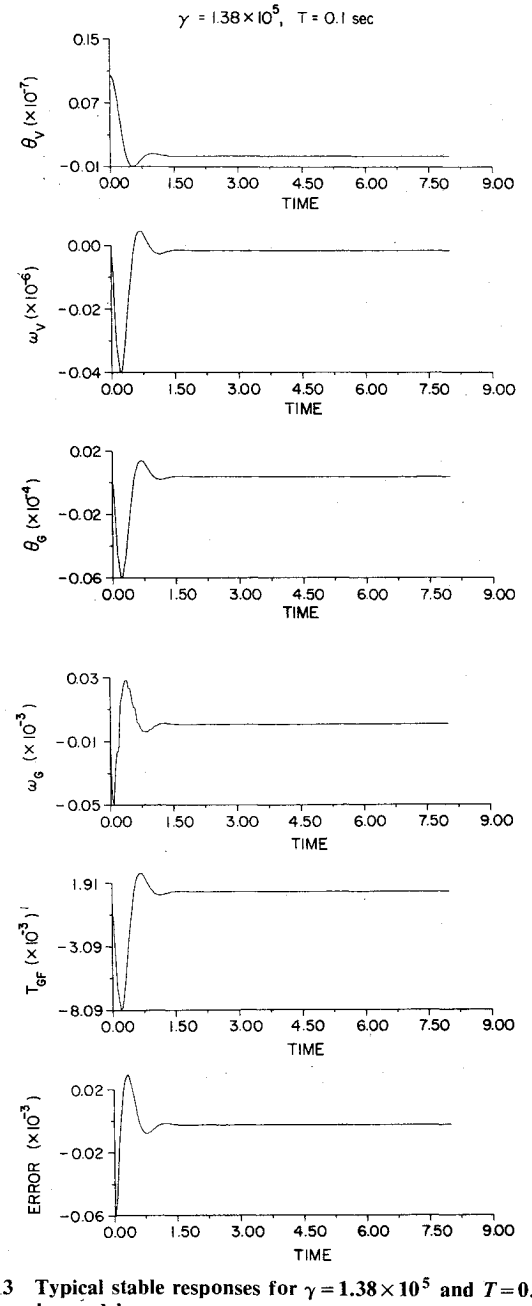

Fig. 13 Typical stable responses for $\gamma = 1.38 \times 10^5$ and $T = 0.1$ sec; one-sampler model.

Theorem 4. *Asymptotic behavior of* $-1/N(z)$ *as A approaches zero.*

$$\lim_{A \to 0} F(z) = -\frac{1}{\gamma T_{GFO}{}^2} \tag{38}$$

for all ϕ and all N.

V. Stability Analysis of the LST

The plots of $-1/N(z)$ together with that of $G(z)$ in the frequency-domain allow the study of the condition of self-sustained oscillations of the sampled-data LST system.

For $N=2$, the expression for $F(z) = -1/N(z)$ is given by Eq. (25). Figure 6 shows the $F(z)$ plot for $N=2$ in the gain-phase coordinates with $0 \leq A < \infty$ and various values of ϕ. The value of γ is 1.38×10^5. Note that the plot stays on the $-180°$ and $-360°$ axes.

In general, $N(z)$ for $N \geq 3$ is given by Eq. (29). Figure 7 shows the gain-phase plot for $F(z)$ when $N=3$. The curves for several values of ϕ are plotted to illustrate the effect of varying the phase of the input signal to the nonlinearity. It should be noted the phase of the input signal to the nonlinearity. It should be noted that the values of $F(z)$ repeat every $60°$ starting from $\phi = 0°$. As the magnitude of the input signal, A, approaches infinity, the bounds of $F(z)$ are at $-240°$ and $-300°$. Figures 8 and 9 illustrate the $F(z)$ plots for $N=4$ and $N=5$, respectively. For $N=4$, the $F(z)$ plot extends from $-315°$ to $-225°$, and for $N=5$, the span is from $-288°$ to $-252°$.

For stability analysis, it is sufficient to consider only the bounds of the $F(z)$ plot for a fixed N. Self-sustained oscillations characterized by N may occur if $G(z)$ intersects with any part of the $F(z)$ plot. The region bounded by all the $F(z)$ curves for a given N is defined as the "critical region." In Fig. 10 the critical regions for other values for $N=50$ and $N=\infty$ are shown. The general shape of the critical regions for other values of N is easily visualized. Furthermore, Theorems 3 and 4 on the asymptotic behavior of $F(z)$ as $A \to \infty$ and $A \to 0$ are useful in generating the critical regions. It can be proved that as N approaches infinity, $F(z)$ approaches the negative inverse of the describing function of the nonlinearity with continuous-data.[6]

Figures 11 and 12 illustrate the gain-phase plots of $G(z)$ of Eq. (13) with the transfer functions and system parameters as defined in the Nomenclature.

Since these plots are to be used for predicting the existence of self-sustained oscillations in the discrete-data system, the frequency of oscillations is expressed as an integral multiple of the sampling period T. Thus, the frequency of oscillation is represented as

$$\omega_c = \frac{2\pi}{NT} \tag{39}$$

for $N=2, 3, \ldots$

The various plots of each system correspond to different values of N, with T as a parameter. Figure 11 is for small values of T whereas Fig. 12 is for larger values of T.

Notice that for large N and small T, the $G(z)$ curves approach that of the continuous system transfer function $G(s)$; that is, when all samplers are absent.

Superimposing the $G(z)$ plots of Figs. 11 and 12 on the $-1/N(z)$ plots shows that for $\gamma = 1.38 \times 10^5$, self-sustained oscillations will not exist if T is less than 0.25 seconds approximately. For larger values of γ the $-1/N(z)$ plots shift downward proportionally. Thus, with $\gamma = 1.38 \times 10^7$ the lowest point in the $-1/N(z)$ curves becomes approximately -102 db, yielding a system in which self-sustained oscillations will always exist for any sampling period. The periods of these oscillations depend on the sampling period used.

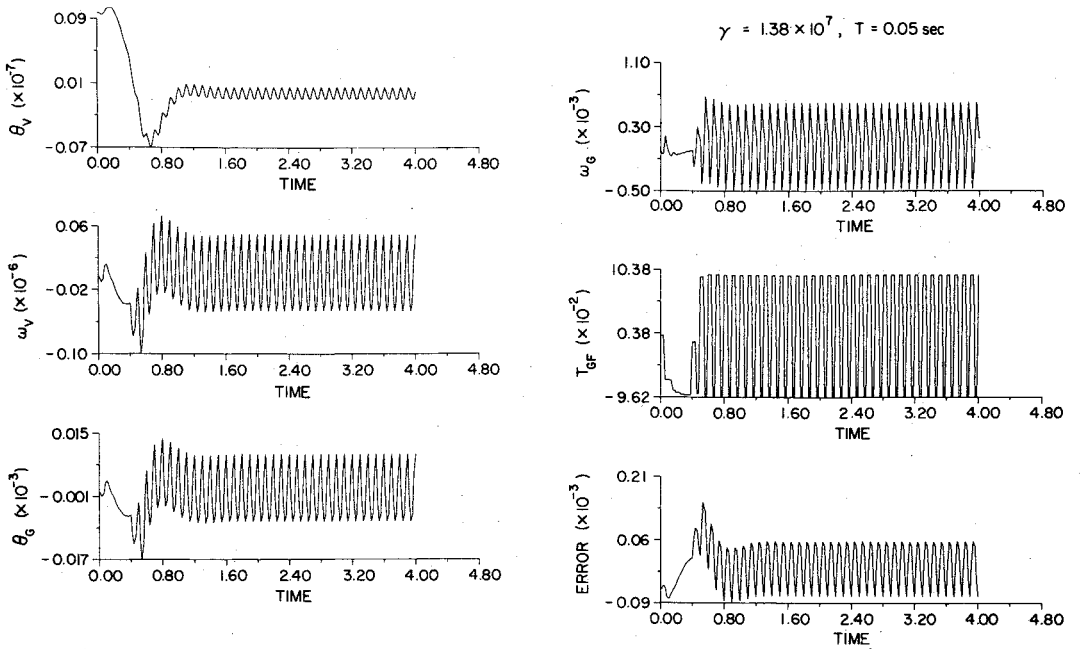

Fig. 14 Typical self-sustained oscillations for $\gamma = 1.38 \times 10^7$ and $T = 0.05$ sec; one-sampler model.

VI. Computer Simulation of the Discrete-Date LST System

A computer simulation of the LST system is presented here to corroborate the results of the discrete describing function analysis. Since the analysis has been carried out with the analytical torque expressions for the CMG frictional nonlinearity, the simulation model of the nonlinearity also has the same characteristics.

Although for analytical convenience the discrete describing function analysis has been carried out with two samplers present in the system, the acutal system has only one sampler. This is at the input to the CMG gimbal drive and there is no sampler in the nonlinearity loop. Consequently, the simulations have been performed with the two-sampler as well as the one-sampler system models. The numerical values used in the simulation model correspond to those given in the Nomenclature.

For the computer simulation, the input to the LST control system, χ, is set to zero, along with the initial states, except for the vehicle position θ_V. the variables measured in the simulations are, θ_V, ω_V, θ_G, ω_G, T_{GF}, and Error (error input command to the CMG). Several sampling periods from $T = 0.005$ sec up to $T = 0.25$ sec are used for both the one-sampler and the two-sampler system simulation models. Simulation results show that with $\gamma = 1.38 \times 10^5$, since the critical regions of the nonlinearity do not intersect with the $G(z)$ plot, for these sampling periods, the system is stable, and no self-sustained oscillations exist. Figure 13 illustrates a typical set of stable responses of the system. When the value of γ of the nonlinearity is increased to 1.38×10^7, a good portion of the $G(z)$ plots in Fig. 12 overlap with the $-1/N(z)$ critical regions, and self-sustained oscillations of all types are possible for the range of sampling periods given above. The details of the simulation parameters and the oscillation periods are shown in Table 1. Note that the one-sampler and two-sampler system models always oscillate with periods close to those which are predicted by the $-1/N(z)$ and $G(z)$ plots. Although the two-sampler model is in closer agreement with the theoretical predictions, these results do justify the approxiamtion of introducing the sampler. Note also that for some sampling periods (e.g., 0.02 sec) although the one-sampler model and the two-sampler model oscillate with periods which differ considerably (0.04 sec and 1.76 sec, respectively) both periods are in fact predicted by the theory.

Figure 13 shows a typical set of stable response for the condition of $\gamma = 1.38 \times 10^5$ and $T = 0.1$ sec with the one-sampler model.

Figure 14 shows a typical set of self-sustained oscillations for the condition of $\gamma = 1.38 \times 10^7$ and $T = 0.05$ sec with the one-sampler model.

From the standpoint of self-sustained oscillations, if γ is at its nominal value of 1.38×10^5, any sampling period less than 0.25 sec approximately should yield a stable system.

Table 1 Computer simulations with $\gamma = 1.38 \times 10^7$

Simulation number	No. of samplers in system model	Sampling period T(sec)	Initial value of θ_V (rad)	Oscillation period (sec) (NT)
1	2	0.005	1.0×10^{-8}	1.58 (316T)
2	1	0.005	1.0×10^{-8}	1.88 (376T)
3	2	0.02	1.0×10^{-7}	0.04 (2T)
4	2	0.02	Continuation of no. 3	0.04 (2T)
5	1	0.02	5.0×10^{-8}	1.76 (88T)
6	2	0.05	1.0×10^{-8}	0.1 (2T)
7	1	0.05	1.0×10^{-8}	1.25 (25T)
8	2	0.1	1.0×10^{-8}	1.0 (10T)
9	1	0.1	1.0×10^{-8}	1.2 (12T)
10	2	0.25	1.0×10^{-7}	0.5 (2T)
11	1	0.25	1.0×10^{-7}	0.75 (3T)

However, other practical considerations and stability considerations due to non-zero inputs would limit the sampling period to a much lower value.

Conclusions

The discrete describing function technique has been applied to the fine-pointing stability study of the Large-Space Telescope (LST). The LST control represents a unique problem in that the fine-pointing stability of the system must be kept within 0.005 arc-sec during the operation of the telescope which sometimes shall last for several hours. Because of the fine-pointing accuracy requirement, the nonlinear friction characteristics of the CMG's must be considered and modeled accurately. An analytical expression for the gimbal friction characteristics has been derived for small-signal analysis.

For the discrete describing function analysis, the input signal to the nonlinearity is assumed to be sinusoidal. Since the nonlinearity is described by an analytical expression, it is possible to derive a closed-form expression for the discrete function. This is a great advantage over the results reported on relay-type and other amplitude-dependent nonlinearities. The intersection between the critical regions generated by the DDF and the linear transfer function $G(z)$ indicate the possibility of a self-sustained oscillation which is characterized by the particular mode. It is shown that for the nominal values of the system parameters, the nonlinear system is stable for reasonably high sampling rates. The graphical technique can be used for design purposes by indicating how the $G(z)$ curve should be reshaped to avoid oscillations.

References

[1] O'Dell, C. R., "Optical Space Astronomy and Goals of the Large Space Telsecope," *Astronautics and Aeronautics*, Vol. 11, April 1973, pp. 22-27.

[2] Osborne, N. A., "Fine Pointing Improvement by Augmentation Methods," AIAA Paper 73-868, Key Biscayne, Fla., 1973.

[3] Dahl, P. R., "A Solid Friction Model," Aerospace Corporation, El Segundo, Calif., TOR-158 (3107-18?-1, May 1968.

[4] Kuo, B. C., *Analysis and Synthesis of Sampled-Data Control Systems*, Prentice-Hall, Inc., Englewood Cliffs, N.J., 1963.

[5] "Forced Oscillations and Suppression of Oscillations in Nonlinear Sampled-Data Systems," *IEEE Transactions on Automatic Control*, Vol. AC-11, April 1966, pp. 290-292.

[6] Kuo, B. C., Seltzer, S. M., and Singh, G., "Stability Study of the Large Space Telescope (LST) System with Nonlinear Friction," AIAA Paper 74-874, Anaheim, Calif., 1974.

[7] Kuo, B. C. and Singh, G., "Continuous and Discrete Describing Function Analysis of the LST System," NASA Contract NAS8-29853, Final Report, George C. Marshall Space Flight Center, Huntsville, Ala., Jan. 1974.